tion from extended-face crystals containing defects, strain and compositional variations. The most practical application of the equations is to supplement the results of kinematical calculations near the Bragg angle.

References

BECKER, P. J. & AL HADDAD, M. (1989). *Acta Cryst.* A**45**, 333–337.

BECKER, P. J. & AL HADDAD, M. (1990). *Acta Cryst.* A**46**, 123–129.

BECKER, P. J. & AL HADDAD, M. (1992). *Acta Cryst.* A**48**, 121–134.

BENSOUSSAN, S., MALGRANGE, C. & SAUVAGE-SIMKIN, M. (1987). *J. Appl. Cryst.* **20**, 222–229.

BRAND, L. (1966). *Differential and Difference Equations*. New York: Wiley.

DAVIS, T. J. (1991). *Aust. J. Phys.* **44**, 693–704.

DAVIS, T. J. (1992). *Acta Cryst.* A**48**, 872–879.

DAVIS, T. J. (1993). *Acta Cryst.* A**49**, 755–762.

EPELBOIN, Y. & AUTHIER, A. (1983). *Acta Cryst.* A**39**, 767–772.

FORSYTH, A. R. (1943). *A Treatise on Differential Equations*, 6th ed. London: MacMillan.

KATO, N. (1980). *Acta Cryst.* A**36**, 763–769, 770–778.

KENDALL, M. G. & STUART, A. (1969). *The Advanced Theory of Statistics*, Vol. 1, 3rd ed. London: Griffin.

KULDA, J. (1987). *Acta Cryst.* A**43**, 167–173.

KULDA, J. (1988). *Acta Cryst.* A**44**, 283–285, 286–290.

PRESS, W. H., FLANNERY, B. P., TEUKOLSKY, S. A. & VETTERLING, W. T. (1987). *Numerical Recipes: the Art of Scientific Computing*. Cambridge Univ. Press.

RISKEN, H. (1984). *The Fokker–Planck Equation: Methods of Solution and Applications*. Berlin: Springer.

SCHNEIDER, J. R., BOUCHARD, R., GRAF, H. A. & NAGASAWA, H. (1992). *Acta Cryst.* A**48**, 804–819.

TAKAGI, S. (1962). *Acta Cryst.* **15**, 1311–1312.

TAKAGI, S. (1969). *J. Phys. Soc. Jpn*, **26**, 1239–1253.

TAUPIN, D. (1964). *Bull. Soc. Fr. Minéral. Cristallogr.* **87**, 469–511.

UHLENBECK, G. E. & ORNSTEIN, L. S. (1930). *Phys. Rev.* **36**, 823–841.

VAN KAMPEN, N. G. (1976). *Phys. Rep.* **24**, No. 3, 171–228.

ZACHARIASEN, W. H. (1967). *Acta Cryst.* **23**, 558–564.

Acta Cryst. (1994). A**50**, 231–238

Long-Period Modulated Structures of $Bi_2Sr_2(Ca_{1-x}Pr_x)Cu_2O_{8+\delta}$ Ceramics Studied by Electron Diffraction and High-Resolution Electron Microscopy

BY T. ONOZUKA

Institute for Materials Research, Tohoku University, Sendai 980, *Japan*

AND Y. HIROTSU

Nagaoka University of Technology, 1603-1 *Kamitomioka, Nagaoka* 940-21, *Japan*

(*Received* 17 *March* 1993; *accepted* 9 *August* 1993)

Abstract

Seven specimens of $Bi_2Sr_2(Ca_{1-x}Pr_x)Cu_2O_{8+\delta}$ ceramics in the concentration range $0 < x < 0.64$ have been prepared by solid-state reaction. The sample with $x = 0.16$ was examined in detail by means of electron diffraction and an intensity distribution of lattice reflections in reciprocal space was constructed on the basis of the experimental results. The intensity distribution is consistent with a calculation using a long-period modulated-structure (LPMS) model. This model with $b = 37b_0$ takes the $(3,1)_5$ mode of lattice modulation having the modulation period $2.31b_0$ (1.25 nm). The period is defined as the reciprocal of the wave number of a satellite reflection. The specimens with other concentrations also showed an intensity distribution of lattice reflections similar to that of $x = 0.16$. On the basis of the above results, lattice modulation periods have been examined for all the prepared specimens. The period decreases roughly from $\sim 1.2_8$ to $\sim 1.1_5$ nm with increasing concentration x. Seven modulation modes of the lattice have been determined by high-resolution observation; the modulation period of the LPMS model with each modulation mode is also nearly equal to the measured period.

1. Introduction

The superconducting ceramic $Bi_2Sr_2CaCu_2O_{8+\delta}$ has large lattice modulations along the b and c axes. Its basic structure is of the $Bi_4Ti_3O_{12}$ type with repeat b_0 (Fig. 1), having an orthorhombic lattice of unit-cell dimensions $a = a_0$, $b = b_0$ and $c = c_0$ ($a_0 \simeq b_0 \simeq 0.54$ and $c_0 \simeq 3$ nm). The lattice constants are taken as $a_0 = 2^{1/2}a_t$, $b_0 = 2^{1/2}a_t$ and $c_0 = 2c_t$, where a_t and c_t represent the values of the $Bi_4Ti_3O_{12}$-type structure.

The modulated structure has been intensively investigated by electron diffraction and high-resolution electron microscopy by Shaw, Shivashankar, La Placa, Cuomo, McGuire, Roy, Kelleher &

Yee (1988), who first found the existence of the striking lattice modulations in the crystal, which lead to a large decay in the intensities of superlattice reflections. Matsui, Maeda, Tanaka & Horiuchi (1988) have observed in a [100] high-resolution image a strong contraction and a compensating expansion of lattice spacing, which result in fluctuations of the spacings $c_0/4$ and $2.5b_0$. A structural model of $b = 5b_0$ constructed by Hirotsu, Tomioka, Ohkubo, Yamamoto, Nakamura, Nagakura, Komatsu & Matsushita (1988) according to contrast modulations of [100] and [010] high-resolution images and electron-diffraction experiments allows recognition of a large decay in the intensity of the superlattice reflection comparable with observation. In addition to the above contrast modulations, a one-dimensional contrast modulation along the b axis has been observed in a [001] high-resolution image (Hewat, Bordet, Capponi, Chaillout, Hodeau & Marezio, 1988).

With increasing substitution of yttrium for calcium in the superconducting ceramic, the period of lattice modulation along the b axis decreases, the decrease in period being attributed to an increase of the mixing ratio of domains of period $4b_0$ rather than $5b_0$ with domains of period $4.5b_0$ in a LPMS model (Onozuka, Iwabuchi, Fukase, Saito & Mitchell, 1991). Furthermore, the mixing mode of the two domains (lattice-modulation mode) has been recognized from photometric measurements of the density distribution of the one-dimensional contrast modulation (Onozuka, 1993).

Intensive studies of the superconducting ceramic with $x = 0$ have also been conducted by X-ray and neutron diffraction, the data being analysed by a method for the refinement of the modulated structure of the ceramic (Gao, Coppens, Cox & Moodenbaugh, 1993; Yamamoto, Onoda, Takayama-Muromachi, Izumi, Ishigaki & Asano, 1990). This analytical method is based on the assumption that the periodicity of the modulation wave is an irrational multiple of the basic lattice repeats of the crystal (intrinsically incommensurate modulation).

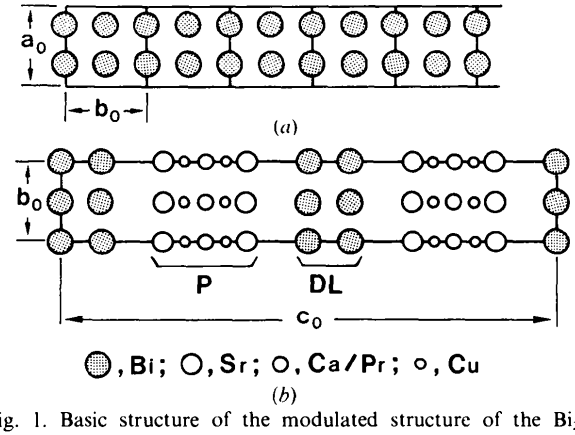

Fig. 1. Basic structure of the modulated structure of the $Bi_2Sr_2(Ca_{1-x}Pr_x)Cu_2O_{8+\delta}$ substitutional system: (*a*) [001] projection, showing the arrangement of a square mesh of metal atoms, $(a_0/2) \times (b_0/2)$; (*b*) [100] projection. The grey circles represent Bi atoms. The large, medium and small open circles represent Sr, Ca/Pr and Cu atoms, respectively, and *P* and DL indicate perovskite-type structure and bismuth double layers, respectively. O atoms are not shown.

In this study, we start from the different standpoint that it is possible to detect the modulated structure of the $Bi_2Sr_2(Ca_{1-x}Pr_x)Cu_2O_{8+\delta}$ system as a commensurate one using current experimental techniques. This is based on experimental findings proving the existence of long-period units in the crystal (Onozuka *et al.*, 1991; Onozuka, 1993). The purpose of the present work is to verify whether the intensity distribution of lattice reflections and the lattice-modulation mode of $Bi_2Sr_2(Ca_{1-x}Pr_x)Cu_2O_{8+\delta}$ ceramics agree with the LPMS model.

2. Experimental

Specimens were prepared by solid-state reaction from mixtures of Bi_2O_3, $SrCO_3$, $CaCO_3$, Pr_6O_{11} and CuO powders, which had metal-atom compositions $BiSr_2(Ca_{1-x}Pr_x)Cu_2$ with $x = 0.08n$ ($n = 0$, 1, 2, 4, 6, 7 and 8). Each initial mixture was carefully ground for about 2 h in a mortar. Then the mixtures were prefired at 1123 K in air for about 12 h. The heating rate from 1023 to 1123 K was 10 K h^{-1}. The prefired mixtures were again ground for about 1 h and then heated again at 1123 and 723 K in air for about 50 and about 5 h, respectively. X-ray powder diffractometry of the specimens was carried out using Philips 1700 X-ray apparatus with Cu $K\alpha$ radiation. X-ray patterns of the specimens with $x = 0.0$, 0.08, 0.16. 0.32 and 0.48 showed the existence of a single-phase $Bi_4Ti_3O_{12}$-type structure, but the specimens with $x = 0.56$ and 0.64 showed weak peaks of an impurity phase whose characterization has not been carried out in this study.

Electron-diffraction experiments were carried out on specimens prepared by ion-milling and crushing methods using electron microscopes equipped with top- and side-entry stages (JEM-200CX and JEM-2000EX). A selected aperture of 20 μm was adopted, corresponding to a hole on the image plate about 0.3 μm in diameter. Wave numbers q of the superlattice reflection, whose reciprocal defines the lattice-modulation period, were obtained from electron-diffraction patterns with [001] incidence magnified 15 times. Observation of the [001] high-resolution images was carried out on cleaved (001) surfaces with a wide field of homogeneous thickness, using a 200 kV electron microscope (JEM-200CX, C_s = 0.8 mm). The specimen was easily prepared by

crushing, since the layered compound $Bi_2Sr_2(Ca_{1-x}Pr_x)Cu_2O_{8+\delta}$ cleaves on a (001) crystal plane. Because of the need for high contrast in the one-dimensional modulations, rather thick fields of the specimens were selected (Onozuka, 1993). About six images per field were taken at defocus intervals of 5 nm around the Scherzer defocus value ($f = -50$ nm) with an exposure time of 2.8 or 4 s and a magnification of 5×10^5.

Photometric density distributions of one-dimensional contrast modulation were directly recorded from negative films of the [001] images using a microphotometer (Sakura, densitometer TDM5). An illumination slit of 15×1100 μm in size was scanned on the film along the b axis at a scanning speed of 0.14 mm min^{-1}. The slit dimensions correspond to an area of 0.03×2.2 nm $[(b_0/18) \times 4a_0]$ on the image.

3. Results

3.1. *Electron diffraction*

The electron-diffraction patterns of Fig. 2 are from the same area of the specimen at different tilt angles around the c axis. The streaks along the c^* axis observed in them are attributed to the existence of local disorder in the (001) stacking sequence in the crystal. Similar streaks are also observed in Fig. 3(*a*). The patterns in Figs. 3(*b*) and (*c*) are cross sections perpendicular to the patterns in Figs. 2 and 3(*a*). Points *B*, *C*, *D* and *F* in Fig. 3(*c*) are equivalent to the points intersected by the line $h = 1$ on the lines OB', OC', OD' and OE', respectively, in Fig. 2(*e*) [*i.e.* point *F* in Fig. 3(*c*) is equivalent to point *E* in Fig. 3(*b*)]. The intensities of reflection spots *A* and *E* in Fig. 3(*b*) and of spots *B* and *D* in Fig. 3(*c*) are caused by streaks: a fine streak crosses at points corresponding to these spots in the patterns shown in Figs. 2(*a*), 3(*a*), 2(*b*) and 2(*d*), respectively.

In addition, spots *B* and *D* in Fig. 3(*c*) are caused by dynamical effects that can, for example, occur between the 040, $0,4-2\Delta,0$, $1,3+2\Delta,0$ and 130 reflections. A rather strong intensity is observed for spot C'' in Fig. 2(*c*). This strong intensity is presumably caused by large dynamical effects between neighbouring reflections along the c^* axis, since the point C'' is equivalent to point *C* in Fig. 3(*c*) and the weak intensity of the reflection spot *C* may be the result of both small dynamical effects and a weak streak crossing at the point *C* along the c^* axis. Besides the above reflection spots, very weak reflection spots *G* and *I* are observed in Fig. 3(*c*).

Even when the concentration x was changed, patterns similar to those of Figs. 2(*a*) and 3(*b*) were obtained but the position of the superlattice reflection spot was shifted slightly along the b^* axis. The intensity distribution of lattice reflections, shown in Fig. 4, was constructed on the basis of the results of Figs. 2 and 3. Very weak reflections [*e.g.* the spots *G* and *I* in Fig. 3(*c*)] are not shown. The *HKL* indices take into consideration the formation of a modulated structure with $b = 9b_0$ in this substitutional system. Reflections are also indexed in Fig. 5(*c*).

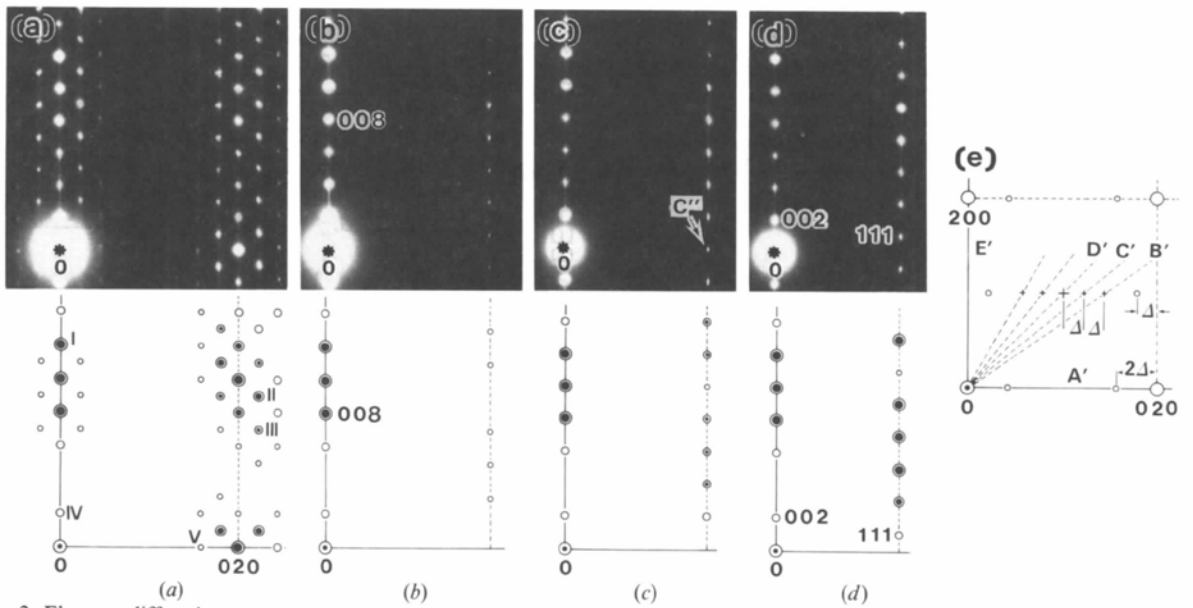

Fig. 2. Electron diffraction patterns ($x = 0.16$) and calculations of reflection intensities: (*a*) [100] pattern; (*b*), (*c*) and (*d*) patterns on reciprocal cross sections including the c^* axis and the broken lines OB', OC' and OD' in (*e*), respectively; (*e*) illustration of a [001] pattern (Fig. 3*b*). Relative intensities I > 100, II > 50, III > 20, IV > 5 and V > 1 are normalized with the intensity of the transmitted beam, $I_0 = 1000$. The *hkl* indexes are based on the basic lattice.

The shift of superlattice reflection spots by changing of the concentration x is shown by the increase of the separation between the weak reflection spots M and N in Fig. 5. The concentration dependence of the wave number q ($=2\Delta$) is examined on the specimens. Then, wave numbers q are derived by measuring the distances between the $0, \pm(2+2\Delta), 0$ and $0, \pm(2-2\Delta), 0$ reflection spots with accuracy higher

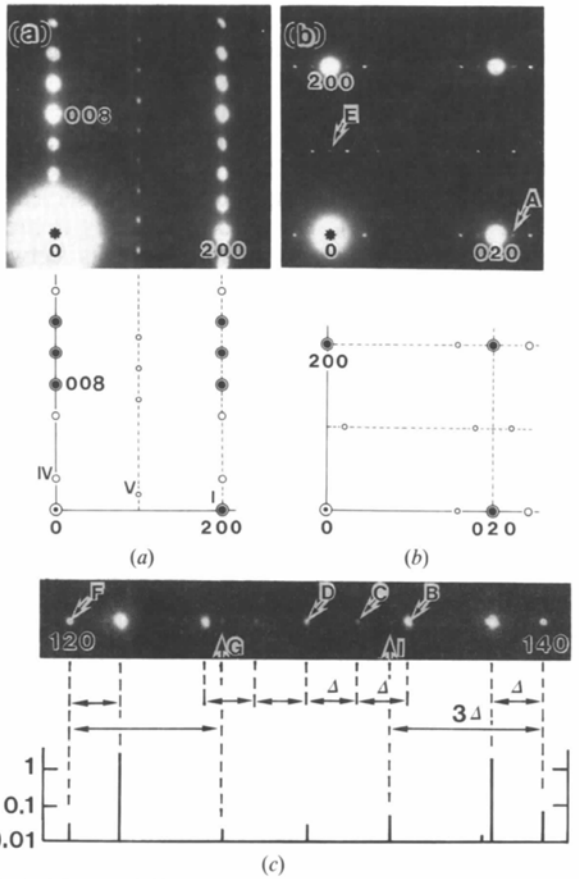

Fig. 3. Electron diffraction patterns ($x = 0.16$) and calculation of reflection intensities: (*a*) [010] incidence, (*b*) [001] incidence, (*c*) pattern between the 120 and 140 reciprocal points. Relative intensities in (*a*) and (*b*) are shown in the same way as those of Fig. 2 and those of (*c*) on a logarithmic scale. The *hkl* indices are based on the basic lattice.

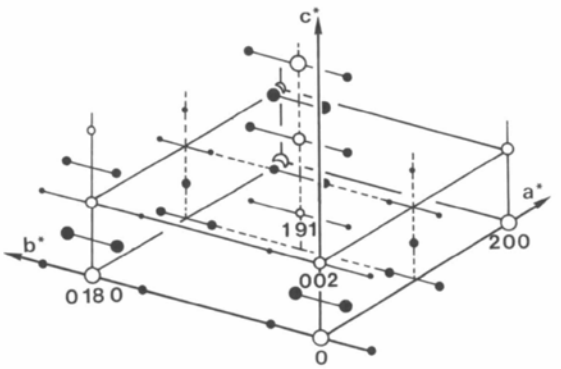

Fig. 4. Intensity distribution of lattice reflections. Open circles represent fundamental reflection spots and solid ones superlattice reflection spots. The *HKL* indices are based on the lattice of unit-cell dimensions $a = a_0$, $b = 9b_0$ and $c = c_0$.

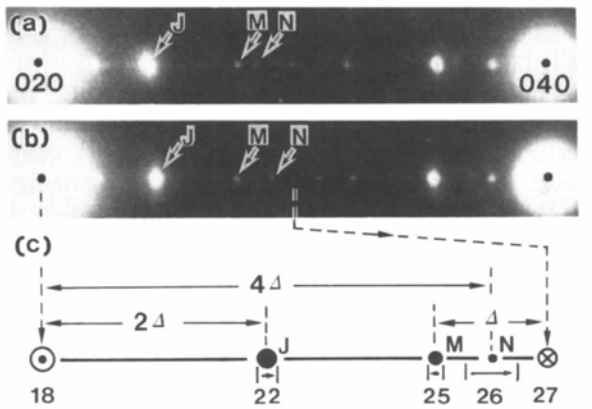

Fig. 5. Electron diffraction patterns between the 020 and 040 reflections: (*a*) $q = 0.43_2 b_0^*$ ($x = 0.08$), (*b*) $q = 0.45_7 b_0^*$ ($x = 0.56$) and (*c*) schematic drawing of (*a*) and (*b*) at double the scale along the b axis. The solid circles represent superlattice reflection spots. The spots shift in the directions of the arrows with x within these ranges with the ends at both sides of each spot. The numeral under the spot is the K index based on the lattice of unit-cell dimensions $a = a_0$, $b = 9b_0$ and $c = c_0$.

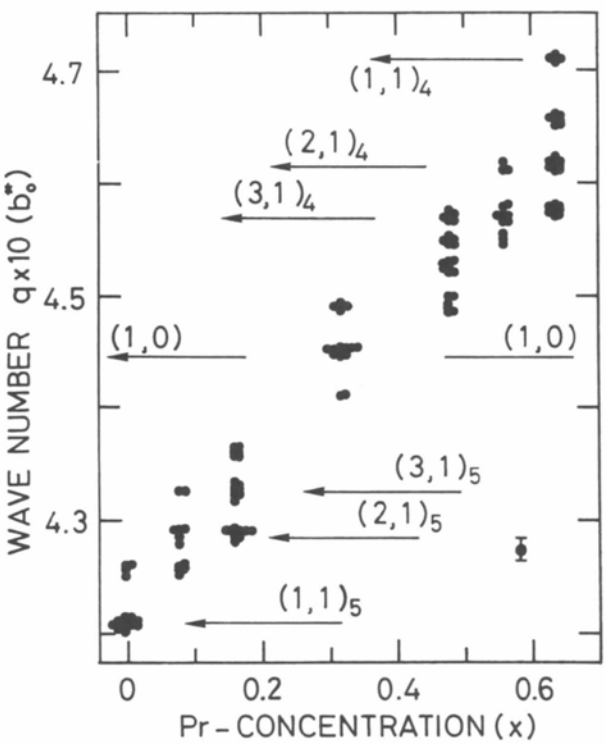

Fig. 6. A plot of wave number q against praseodymium concentration x. Some wave numbers q_c are indicated by arrows with their $(N_I, N_{II})_{\Lambda_{II}}$ modes.

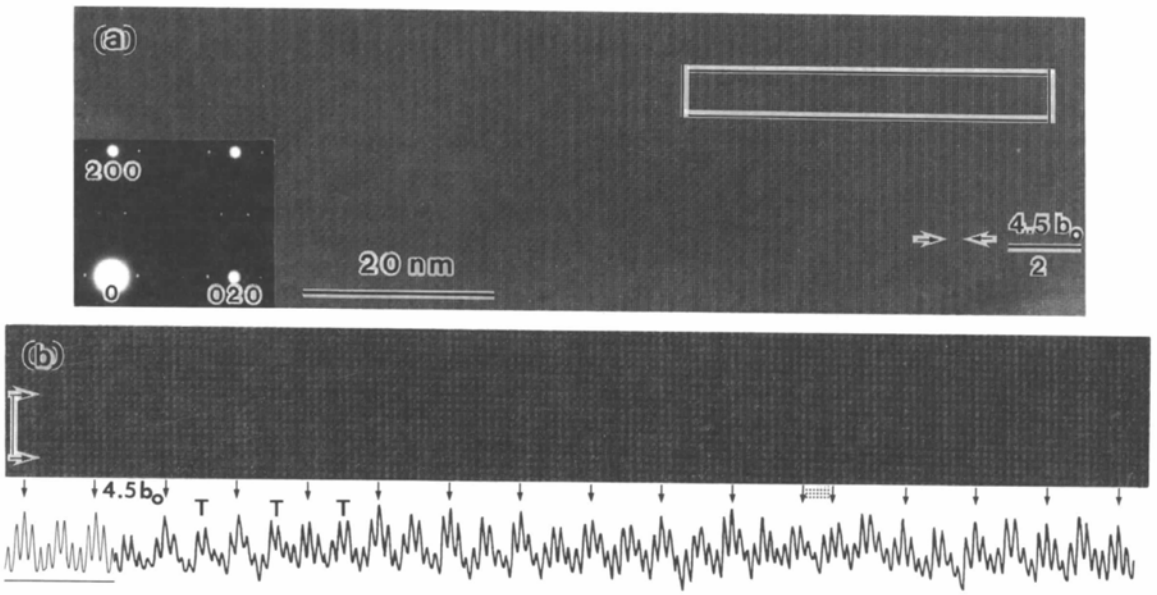

Fig. 7. (*a*) [001] high-resolution image of the structure of $q = 0.44_4 b_0^*$ ($x = 0.32$) and its electron-diffraction pattern. (*b*) Enlargement of the rectangular part in (*a*) and its microphotometric density-distribution curve with the simulation on the left. The scanning zone of the slit of the microphotometer is shown by the two arrows along the *b* axis.

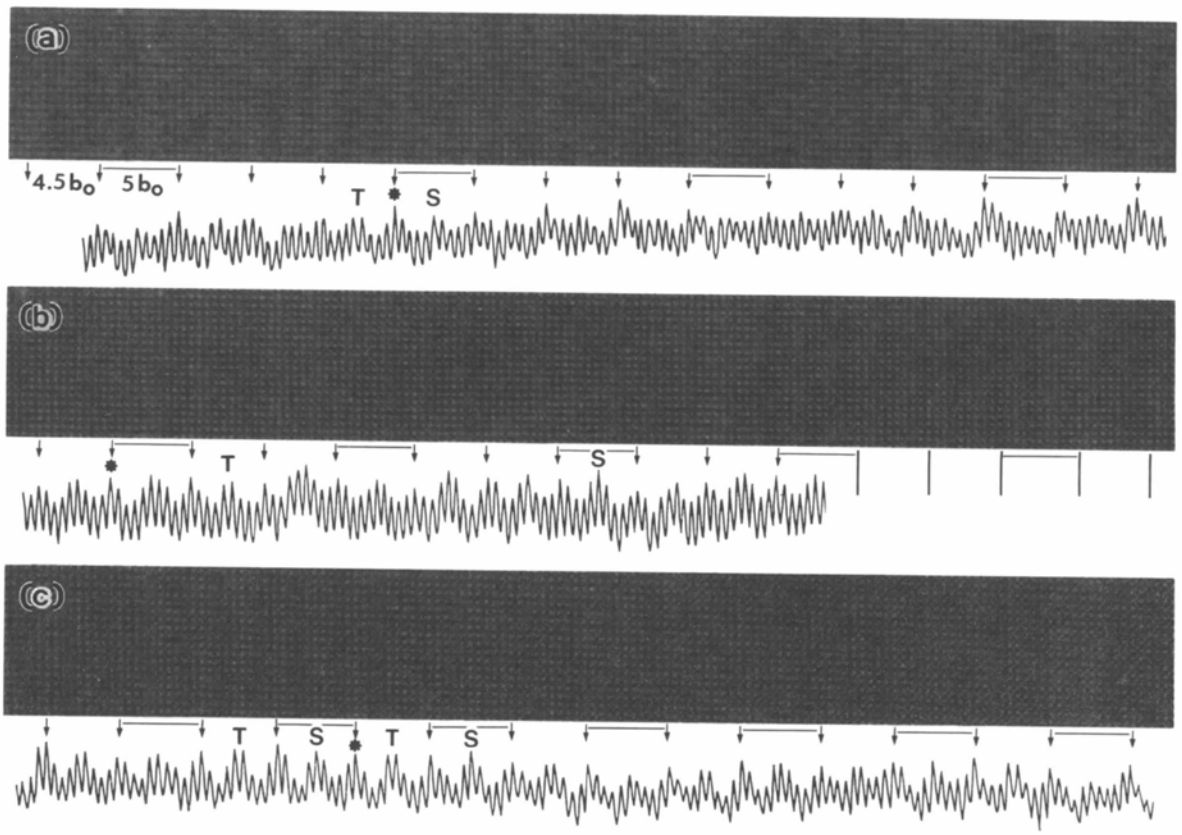

Fig. 8. [001] high-resolution images and their microphotometric density-distribution curves: (*a*) $q = 0.43_2 b_0^*$ ($x = 0.16$), (*b*) $q = 0.42_9 b_0^*$ ($x = 0.08$) and (*c*) $q = 0.42_1 b_0^*$ ($x = 0$).

than 0.05 mm (see Fig. 2*e*).† This accuracy corresponds to an error range of $\pm 0.001 b_0^*$ (the bar in Fig. 6) for the measured values of q plotted in Fig. 6. Here, b_0^* represents the reciprocal of b_0.

The wave number of Fig. 6 increases roughly linearly and seems to show a stepwise increase with the increase in x: behaviour similar to the case of the substitutional element Y. The experimental points for each concentration x are, however, divided into a few small groups. For example, the points on $x = 0.32$ make three groups around the values $0.440 b_0^*$, $0.444 b_0^*$ and $0.449 b_0^*$. The presence of a group of q values instead of a single value may be attributed to the non-homogeneity of composition in specimens.

The points in the middle group on $x = 0.32$ lie in the hypothetical error range $0.443 b_0^*$–$0.445 b_0^*$ to the wave number $0.444 b_0^*$ ($4 b_0^*/9$) of the 040 reflection of the modulated structure with $b = 9 b_0$ described before. This coincidence allows one to take the modulated structure as one corresponding to the middle group of points. This structure is a basic one for the modulated structures of this substitutional system.

† Deviation of less than 2° of the modulation vector from the b^* axis was observed on electron-diffraction patterns with [001] incidence with a probability of about 1/10. A corresponding deviation was also observed in the [001] high-resolution image, as seen in Figs. 7(*b*) and 8(*c*).

3.2. *High-resolution electron microscopy*

The [001] high-resolution image in Fig. 7(*a*) exhibits a one-dimensional contrast modulation with an approximate period $4.5 b_0/2$ along the b axis. The details of the contrast modulation are observable in the photometric density distribution in Fig. 7(*b*), where a single maximum peak marked by an arrow occurs once every nine peaks ($4.5 b_0$). Short units of density distribution, $4.5 b_0 (b_1)$, have twin peaks in the middle and are double the approximate period of the contrast modulation in Fig. 7(*a*). This density distribution, showing repetition of the unit b_1, is a basic one among those of the substitutional system.

Short units of density distribution, $5 b_0 (b_2)$ and $4 b_0 (b_3)$, appear as new periodicities in alignments of unit b_1. The former unit is found in the photometric density-distribution curves of lower concentrations shown in Fig. 8; the latter in those of higher concentrations shown in Fig. 9. Arrows on these curves show single maximum peaks every nine (b_1), ten (b_2)

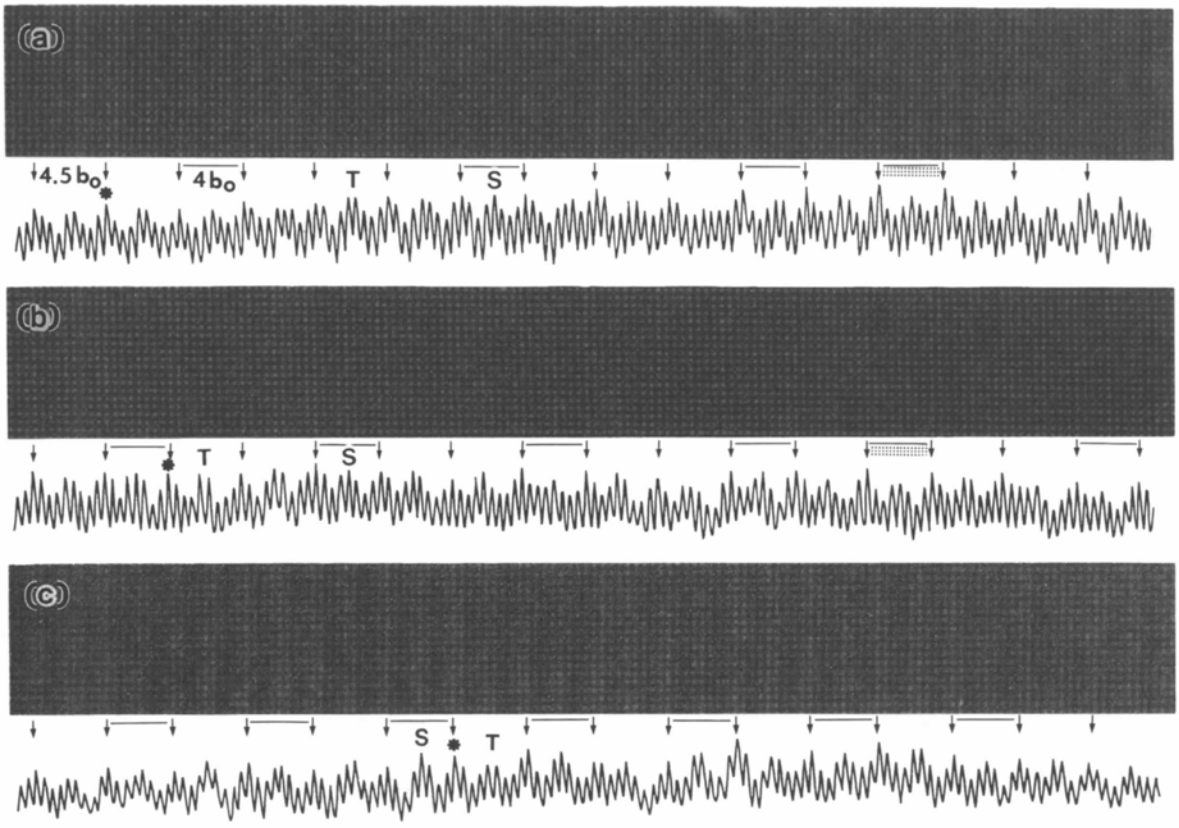

Fig. 9. [001] high-resolution images and their microphotometric density-distribution curves: (*a*) $q = 0.45_8 b_0^*$ ($x = 0.54$), (*b*) $q = 0.46_2 b_0^*$ ($x = 0.64$) and (*c*) $q = 0.47_1 b_0^*$ ($x = 0.64$).

or eight peaks (b_3) from the starting peak marked by an asterisk. The units b_2 and b_3 are located by a horizontal line. Typical examples of density-distribution units b_1 and b_2 or b_3 are indicated by the letters T and S, respectively. The units b_2 and b_3 take a single maximum peak at the middle in contrast to the twin peaks of the unit b_1. The single maximum peak has subpeaks on each side.

It was shown in the previous paper (Onozuka, 1993), focused on computer simulations, that such periodic alignments of unit b_1, units b_1 and b_2 or b_1 and b_3 can be described in terms of the $(N_{\rm I}, N_{\rm II})_{\lambda_{\rm II}}$ mode of lattice modulation of the LPMS model. The simulation has displayed a symmetrical distribution of peak intensities at the middle of units of $4.5b_0$, $5b_0$ and $4b_0$ (*e.g.* the inset in Fig. 7*b*). Here, $N_{\rm I}$ and $N_{\rm II}$ are taken, respectively, as the number of units b_1 and b_2 or b_1 and b_3 included in a long-period unit in photometric density distributions. The subscript $\lambda_{\rm II}$ is 5 or 4, corresponding to a unit b_2 or b_3 in the long-period unit, respectively. The photometric density distributions of Figs. 7, 8 and 9 reveal the existence of the (1,0), $(3,1)_5$, $(2,1)_5$, $(1,1)_5$, $(3,1)_4$, $(2,1)_4$ and $(1,1)_4$ modes in the corresponding crystal. These modes are shown in Fig. 6 for each wave number q.

According to the LPMS model, the wave number q corresponding to the $(N_{\rm I}, N_{\rm II})_{\lambda_{\rm II}}$ mode can be expressed as

$$q_c = [2(N_{\rm I} + N_{\rm II})/(4.5N_{\rm I} + \lambda_{\rm II}N_{\rm II})](b_0^*), \qquad (1)$$

where $\lambda_{\rm II}$ represents the numeral of the subscript. The wave numbers q_c indicated by arrows in Fig. 6 are derived by substituting in (1) the unique pair of $N_{\rm I}$ and $N_{\rm II}$, and $\lambda_{\rm II}$ in each $(N_{\rm I}, N_{\rm II})_{\lambda_{\rm II}}$ mode. These wave numbers q_c are nearly equal to the average of the measured values in the corresponding small group of points. It is also noteworthy that the wave number $q_c = 0.4210b_0^*$ corresponding to the $(1,1)_5$ mode is nearly equal to the X-ray datum 0.420 (6)b_0^* measured by Gao *et al.* (1993) in the single crystal.

A very weak reflection intensity showing the existence of disorder in the (001) stacking sequence [*e.g.* the spot E in Fig. 3(*b*)] is usually observed in the pattern from a specimen field including the field on which the high-resolution observation was performed. An example of the pattern is inset in the image of Fig. 7(*a*). Some density distributions of units b_1, b_2 and b_3 in Figs. 7, 8 and 9 distort from the symmetrical ones. The distortion may be attributed to the existence of a small amount of local disorder in the stacking sequence or to a small inclusion in the crystal. This was actually observed in a [100] high-resolution image where the sequence of domains in the $(1,1)_5$ type was interrupted locally by an inclusion with a sequence similar to the $(2,1)_5$ type.

4. Application of the LPMS model to the modulated structure of the $Bi_2Sr_2(Ca_{1-x}Pr_x)Cu_2O_{8+\delta}$ system

The LPMS model is constructed from periodic alignments, along the b axis, of the regions I and II that have the structures with $b = 4.5b_0$ and $b = 5b_0$, and $b = 4b_0$, respectively, shown in Fig. 10; the model has the $(N_{\rm I}, N_{\rm II})_{\lambda_{\rm II}}$ mode of lattice modulation. The lattice has unit-cell dimensions $a = a_0$, $b = Bb_0$ and $c = c_0$. Here, B is given by $(4.5N_{\rm I} + \lambda_{\rm II}N_{\rm II})$ for $N_{\rm I}$ an even number and by $2(4.5N_{\rm I} + \lambda_{\rm II}N_{\rm II})$ for $N_{\rm I}$ an odd number. The metal-atom chains along the a, b and c axes are modulated by waves with longitudinal and tranverse wave components similar to those of the structure model of Hirotsu *et al.* (1988).

The coordinates X, Y and Z of individual metal atoms in the model are expressed as

$$X = X_0 + aU_a\{\sin[(2\pi Y_0/\lambda_{{\rm I},B}) + \beta] - \cos(2\pi Z_0)\}, \qquad (2)$$

$$Y = Y_0 + U_b\cos(2\pi Z_0)\sin[(2\pi Y_0/\lambda_{{\rm I},B}) + \beta], \qquad (3)$$

and

$$Z = Z_0 - \tfrac{1}{2}U_c\sin(2\pi Z_0)\{1 + \cos[(2\pi Y_0/\lambda_{{\rm I},B}) + \beta]\}, \qquad (4)$$

where $\lambda_{{\rm I},B} = 4.5/B$ and $\beta = 0$ for region I and

$$\beta = \pm(\pi/9)\{\sin[(\pi Y_0/\lambda_{{\rm II},B}) - (\pi/2) + \beta'] + 1\} \qquad (5)$$

for region II. Here, α in (2) takes the values -1 and $+1$ for metal atoms on the first and second metal-atom layers along the a axis, respectively. The plus and minus signs at the start of (5) are used for the structures with $b = 5b_0$ and $b = 4b_0$ together with $\lambda_{{\rm II},B} = 5/B$ and $\lambda_{{\rm II},B} = 4/B$, respectively. X_0, Y_0 and Z_0 are the coordinates of metal atoms in an unmodulated structure of the long unit cell. U_a, U_b and U_c represent the amplitudes of the displacement waves in units a_0, Bb_0 and c_0, respectively. β' in (5) is an adjustable parameter to connect region I to region II smoothly. Then, region II serves as discommensuration (secondary modulation) in region I.

The two LPMSs in Figs. 10(*a*) and (*b*), corresponding to Figs. 8(*b*) and 9(*b*), have unit lengths $b = 14b_0$ and $b = 13b_0$, respectively. In spite of their small difference, the two structures are formed around both edges of the wide concentration range $0.08 < x < 0.64$, in which several LPMSs are formed (Fig. 6). Here, the coordinates X_0, Y_0 and Z_0 were taken according to those of the average structure determined by Sunshine, Siegrist, Schneemeyer, Murphy, Cava, Batlogg, Van Dover, Fleming, Glarum, Nakahara, Farrow, Krajewski, Zahurak, Waszczak, Marshall, Marsh, Rupp & Peck (1988).

The amplitudes of the displacement waves were taken as $U_a \times a_0 = 0.008$, $U_b \times Bb_0 = 0.045$ and $(U_c \times c_0)/2 = 0.03$ nm. These values were determined from a calculation of the intensity distribution of reflections consistent with the observations (Figs. 2 and 3). The amplitudes 0.045 and 0.03 nm are comparable with those, 0.044 and 0.03 nm, of the isostructural compound $Bi_{10}Sr_{15}Fe_{10}O_{48}$, which has a unit length $b = 5b_0$ (Le Page, McKinnon, Tarascon & Barboux, 1989).

Intensities of lattice reflections for electron diffraction were kinematically calculated from the LPMS models with the lattice-modulation modes determined in this study. The scattering amplitudes for electrons of the metal atoms were approximated by the atomic numbers. The calculation based on the LPMS model with the $(3,1)_5$ mode ($b = 37b_0$) is compared with the observations in Figs. 2 and 3. For example, the $0(H),90(K),0(L)$ reflection with the wave number $q_c = 0.4324b_0^*$ has an appreciable intensity of ~ 10 (Fig. 2*a*). Here, the HKL indices are based on the lattice with $b = 37b_o$ in place of that with $b = 9b_0$ used before and the K interval of 16 corresponds to 2Δ ($= q$). Most of the other $0K0$ reflections have intensities less than ~ 0.02, except those with $K = 58 \pm 2$ and $K = 90 \pm 2$. The reflections corresponding to the weak spots G, I, M and N (Figs. 3*c* and 5) have rather strong intensities, 0.04–0.1, in comparison with other reflections.

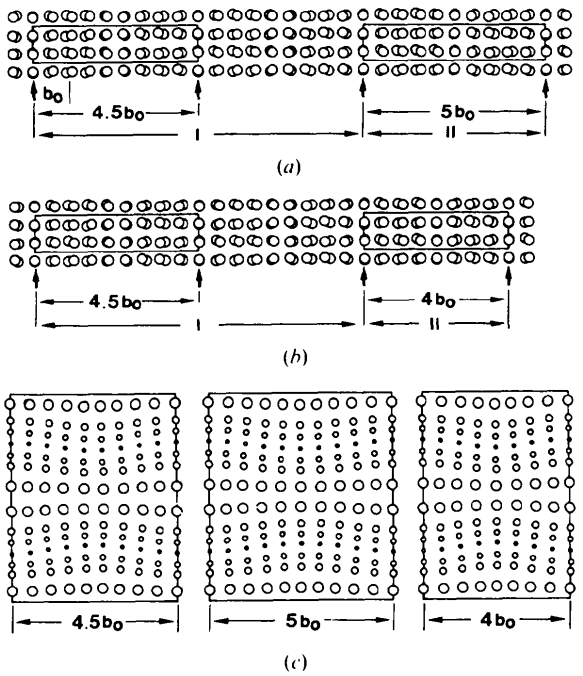

Fig. 10. LPMS model: (*a*) and (*b*) are [001] projections of metal atoms of the models with the $(2.1)_5$ and $(2.1)_4$ modes of lattice modulation, respectively, where only Bi atoms are seen. The rectangles show the three subunit cells, $a_0 \times 4.5b_0 \times c_0$ (the crystallographic unit cell $a_0 \times 9b_0 \times c_0$), $a_0 \times 5b_0 \times c_0$ and $a_0 \times 4b_0 \times c_0$. (*c*) [100] projections of metal atoms in the three subunit cells. The large, medium, small and very small circles represent Bi, Sr, Ca/Pr and Cu atoms, respectively.

The authors gratefully thank Dr G. Pezzotti for proofreading the manuscript and Professor M. Tanaka for his help in the high-precision microphotometric analyses. The authors also thank Professor K. Hiraga for his encouragement during the course of this study. This work was partly supported by a Grant in Aid of Scientific Research from the Ministry of Education, Science and Culture of Japan.

References

GAO, Y., COPPENS, P., COX, D. E. & MOODENBAUGH, A. R. (1993). *Acta Cryst.* A**49**, 141–148.

HEWAT, E. A., BORDET, P., CAPPONI, J. J., CHAILLOUT, C., HODEAU, J. L. & MAREZIO, M. (1988). *Physica (Utrecht)*, C**153–155**, 619–620.

HIROTSU, Y., TOMIOKA, O., OHKUBO, T., YAMAMOTO, N., NAKAMURA, Y., NAGAKURA, S., KOMATSU, T. & MATSUSHITA, K. (1988). *Jpn. J. Appl. Phys.* **27**, L1869–L1872.

LE PAGE, Y., MCKINNON, W. R., TARASCON, J.-M. & BARBOUX, P. (1989). *Phys. Rev. B*, **40**, 6810–6816.

MATSUI, Y., MAEDA, H., TANAKA, Y. & HORIUCHI, S. (1988). *Jpn. J. Appl. Phys.* **27**, L372–L375.

ONOZUKA, T. (1993). *J. Appl. Cryst.* **26**, 104–111.

ONOZUKA, T., IWABUCHI, Y., FUKASE, T., SATO, H. & MITCHELL, T. E. (1991). *Phys. Rev. B*, **43**, 13066–13072.

SHAW, T. M., SHIVASHANKAR, S. A., LA PLACA, S. J., CUOMO, J. J., MCGUIRE, T. R., ROY, R. A., KELLEHER, K. H. & YEE, D. S. (1988). *Phys. Rev. B*, **37**, 9856–9859.

SUNSHINE, S. A., SIEGRIST, T., SCHNEEMEYER, L. F., MURPHY, D. W., CAVA, R. J., BATLOGG, B., VAN DOVER, R. B., FLEMING, R. M., GLARUM, S. H., NAKAHARA, S., FARROW, R., KRAJEWSKI, J. J., ZAHURAK, S. M., WASZCZAK, J. V., MARSHALL, J. H., MARSH, P., RUPP, L. W. JR & PECK, W. F. (1988). *Phys. Rev. B*, **38**, 893–896.

YAMAMOTO, A., ONODA, M., TAKAYAMA-MUROMACHI, E., IZUMI, F., ISHIGAKI, T. & ASANO, H. (1990). *Phys. Rev. B*, **42**, 4228–4239.